

Geologic Mapping of Keping Uplift, Northwestern Margin of the Tarim Basin
Based on Absorption Features Using Hyper-multispectral Image Data

Kinya Okada

Japex Geoscience Institute, Inc.

Tokyo, Japan

Takumi Ohnuma

Japex Geoscience Institute, Inc.

Tokyo, Japan

Hiroshi Watanabe

Japex Geoscience Institute, Inc.

Tokyo, Japan

Abstract. A method for hyper-multispectral remote sensing data is developed, and some test results using Airborne Visible/Infrared Imaging Spectrometer (AVIRIS) and the Geophysical Environmental Research Co. 63-channel Airborne Imaging Spectrometer (GERAIS) data of the Cuprite mining districts are shown. The developed software is applied to GERAIS data acquired in October, 1990 over the eastern part of the Keping Uplift, located in the northwestern margin of the Tarim Basin, China. Several rocks and minerals are identified and mapped, including limestone and dolostone which are well discriminated.

I . Introduction

Laboratory spectra of rocks and minerals were shown to be useful in their discriminations. Most of the remote sensing data from satellites, however, have a limited number of band and it was not easy to identify surface materials in detail. On the other hand, airborne imaging spectrometers to acquire hyper-multispectral image data in the VNIR and SWIR have been developed. For geological mapping, particularly, absorption band imagery extracted from hyper-multispectral image data is shown to be useful because it has an ability to reveal the mineral composition of surface in detail.

Tarim Basin has been geologically investigated using remote sensing data with the cooperation of Chinese Academy of Sciences since 1987. This paper focused on the eastern part of the Keping Uplift, located in the northwestern margin of the Tarim Basin, where Palaeozoic sequences are well exposed. The data was collected by the Geophysical Environmental Research Co. (GER) 63-channel Airborne Imaging Spectrometer. The GER system has a single aperture with three separate spectrometers for three separate detector arrays and spectrally covers approximately from 400 nm to 2500 nm (Collins and Chang, 1988; Table 1). In this paper, we describe the methodology and its application to the Tarim Basin study for rock type discrimination using hyper-multispectral remote sensing data.

II . Methodology

AVIRIS and GERAIS data of the Cuprite mining districts were used as test data. The Cuprite area, located on the western edge of Nevada, is well known as a test site of a lot of airborne sensors. Ashley and Abrams (1980) describe geology, especially hydrothermal alteration of the Cuprite. The hydrothermal alteration areas are divided into three mappable zones: silicified rocks, opalized rocks, and argillized rocks. Opalized rocks contain alunite and kaolinite.

Our approach to spectral processing of hyper-multispectral image data consists of three steps: pre-processing, feature extraction, and

mapping (Okada and Iwashita, 1990). In the first two steps, a raw spectrum from each pixel is processed (Figure 1). The raw spectrum in radiance or digital number (DN) is influenced by several factors such as solar incident energy, atmospheric absorption and scattering, and topographic effects, in addition to the reflectance of surface materials.

Pre-processing converts a raw spectrum to a reflectance(-like) spectrum. For this conversion, a lot of techniques are proposed (Green and Craig, 1985, Kruse, 1988 etc.). In this study, we take a simple way in order to process rapidly a large volume of data. The conversion is accomplished by ratioing a raw spectrum data of each pixel to the average spectrum data over entire image. This process removes major solar radiation and atmospheric effects. However, if a major part of surface materials is homogeneous, this method is not effective, because the average spectrum includes reflectance feature. For the correction of topographic effects, the equal energy normalization is useful, however, this is likely to enhance noise components of very dark areas such as shadows which have low signal-to-noise ratio as well. Therefore, we did not apply the correction of topographic effects. Figure 2 shows a laboratory spectrum of a rock sample collected at Kaolinite Hill where kaolinite rich rocks are exposed and converted spectra of AVIRIS and GERAIS in the corresponding areas. The location and shape of absorption features in those spectra are similar one to the other. In particular, AVIRIS's spectrum shows the doublet feature around 2200 nm very well.

In the next step, we extract absorption features from reflectance(-like) spectrum using hull quotient (Green and Craig, 1985) or hull difference methods and derive six parameters for each absorption (Figure 3): the wavelength (λ), depth (D), width (W), symmetry (S), area (A) and slope of upper hull (θ). As shown in the Figure 3, width and symmetry parameters are defined based on the area of absorption parts. Usually, several absorption features are extracted in this processing. Then, a subindex is assigned to each absorption in decreasing order of depth. That is, wavelength parameter is represented such as $\lambda_1, \lambda_2, \dots$. The hull difference method was applied in the actual processing for airborne data, since the hull quotient is likely to extract noise components as deep absorptions in very dark areas such as shadows. For the parameters except for depth and area, two methods provide mostly similar values.

Both AVIRIS and GERAIS data of the Cuprite were processed in the range of 2000 to 2400 nm as a test. A few absorption features were extracted and parameterized for each pixel. A simple way for mapping is to display six parameter-images based on the computed parameters. Figure 4 shows a set of color-coded parameter-images of AVIRIS for the deepest absorption: $\lambda_1, D_1, W_1, S_1, A_1$ and θ_1 -image. The parameter-images of GERAIS show similar pattern to those of AVIRIS. The λ_1 -image of AVIRIS, however, is distinguishable in absorption band due to its higher spectral resolution than GERAIS.

These six parameter-images are a set of basic image for analysis. The λ_1 -image shows a zoning based on absorption band and enables an analyst to estimate some of surface materials. The D_1 and A_1 -images indicate the distribution with a threshold values meaningfully deep absorption features. If other parameter-images are combined with D_1 -image and/or A_1 -image, parameter-images easy to interpret can be obtained. The W_1, S_1 , and θ_1 -images discriminate absorption features which have the same absorption band. The silicified zone (2250 nm absorption; orange

colored) and outer opalized and argillized zone (2160 to 2200 nm absorption; green to yellow colored) are clearly divided on the λ_1 -image of AVIRIS. Furthermore, the difference of alunite (2160 nm; green colored) and kaolinite absorption band (2220 nm; yellow colored) is detectable. Mixed alunite and kaolinite area is expected to have yellow-green colored area. The W_1 -image shows that alunite patterns of western area are wider than those of eastern area. This may relate to something like mixtures. In further analysis, the deepest absorption parameters should be combined with the second and/or third deepest ones and/or the parameters from other wavelength region such as visible region. An analyst can obtain mineralogical information of his study area using these parameter-images.

III. Application to geological mapping in Yingan Shan area, the Tarim Basin, China

A. Purpose

We have been studying the geology of northern margin of the Tarim basin, China using satellite imagery such as LANDSAT and SPOT since 1987. One result of this investigation shows that satellite imagery is a quite useful tool for geological analysis, especially for the analysis of geological structure. However, generally speaking, lithological information obtained from satellite data are limited, because the bandwidths of the sensors loaded on satellite are too wide for detailed spectral discrimination.

In this paper, we use hyper-multispectral image data with high spectral resolution acquired from aircraft to remotely estimate the lithology of strata exposed at the surface.

The study area is Yingan Shan, the NW margin of the Tarim basin (Figure 5). The results illustrate an approach that is applicable to reconnaissance, especially to geological mapping.

B. Approach

We used following steps to map strata exposed in Yingan Shan area.

1. Field survey to get detailed stratigraphic information and rock samples.

These samples are analyzed by chemical analysis, X-ray diffraction analysis, laboratory spectrum measurement, etc.

2. Acquisition of hyper-multispectral image data using GERAIS.
3. Data processing focused on the absorption wavelength and interpretation of absorption images.

In the following section, we will illustrate one of obtained several results about discrimination of limestones from dolostones distributed in this area.

C. Geological setting

The study area, Yingan Shan, is located in the Keping Uplift which defines the NW margin of the Tarim basin. The structure of Keping Uplift was analyzed using LANDSAT imagery by Nishidai and Berry (1990). Keping Uplift is characterized by thin-skinned imbricate thrusts. Yingan Shan is eastern part of the Uplift, therefore the structure style of the area

basically follows that of Keping Uplift. Thick Palaeozoic sequences are exposed throughout the Uplift (Hu et al., 1965). Uplift occurred during the Variscan orogenic movements. Mesozoic rock is absent (Tian et al., 1985). Palaeozoic sequences in Ying'an Shan consist of Cambrian - lower Permian rocks excluding upper Ordovician and Carboniferous. From stratigraphic point of view, these sequences can be subdivided into three major sedimentation cycles (Hu et al., 1965) :

Cambrian - Ordovician cycle	: predominantly carbonates
Silurian - Devonian cycle	: predominantly terrigenous clastics
Permian cycle	: predominantly terrigenous clastics and carbonates

Approximately 4 km thick of marine and nonmarine strata are exposed in the area (Figure 6).

D. Spectral analysis of hyper-multispectral image data

It is well known that calcite has an absorption near 2330 nm while dolomite has one near 2300 nm (Hunt, 1982). We focused on these absorption features and tried to distinguish limestones from dolostones distributed in the area.

These deepest absorptions of calcite and dolomite in SWIR range must appear at the bands 55 and 53, respectively, in GERAIS hyper-multispectral image data used in this paper. However, because spectral smoothing is applied to data to reduce the influence of the noise, these absorptions will appear at the bands 54 - 56 and 52 - 54, for limestones and dolostones respectively.

Reflectance-like spectra processed from GERAIS data well demonstrate those features. Left image in Figure 7 is a false color image of a part of eastern Ying'an Shan composed of the bands 6, 10 and 17. Center wavelength of these bands correspond to those of LANDSAT TM band 2, 3 and 4, respectively. In this figure, lower Cambrian dolostones are distributed around the area marked by "LINE 356" and middle Ordovician limestones are distributed around the area marked by "LINE 651". Figure 8(a) shows reflectance-like spectra along these image lines (pixel number increases from top to bottom). Figure 8(b) shows positions (bands) of absorptions calculated by the software developed in this study. From the comparison of absorption bands of both image lines, it is recognized that first absorption peaks (λ_1) of "LINE 356" appear near 2300 nm which may be due to dolomite and those of "LINE 651" appear near 2330 nm due to calcite. And in lower half of "LINE 651" of Figure 8(b), second absorption peaks (λ_2) appear around 2150 nm, which correspond to second absorption peak of calcite.

Right image in Figure 7 is λ_1 -image superimposed on band 17. In this image, bluish color represent the area where limestones are distributed and greenish color represent that of dolostones. This result well corresponds to distribution of limestones and dolostones observed by the field survey.

The result of this study illustrates that λ_1 -image produced from GERAIS data can be interpreted for the classification of limestones and dolostones. And also, clastic rocks may be able to be mapped as well as carbonate rocks using the software developed in the study. When combined with satellite imagery such as LANDSAT or SPOT, λ_1 -image allows us to make accurate geological maps including mineralogical and lithological information.

IV. Conclusions

We proposed a technique for extracting six parameters to represent absorption features. This parameterization reduces a huge volume of image data with a lot of bands to a few parameter-images. In other words, it is a compression technique to display absorption features.

In the application of Tarim Basin, several minerals were identified and mapped using the parameter-images from GERAIS. Limestone and dolostone were clearly differentiated by detecting a slight shift of their absorption features. And the capability of hyper-multispectral data about rock type discrimination is well demonstrated.

References

- Ashley, R. P. and Abrams, M. J. (1980)
Alteration Mapping Using Multispectral Images - Cuprite Mining District, Esmeralda County, Nevada, U. S. Geological Survey Open File Report, 80-367
- Collins, W. E. and Chang S. (1988)
Application of Geophysical Environmental Research (GER) Airborne Scanner data for detection of hydrothermal alteration in NEVADA, Proceedings of the sixth Thematic conference of Remote Sensing for Exploration Geology, Houston, Texas, Environ.Res. Inst. Michigan, p. 123
- Green, A. A. and Craig, M. D. (1985)
Analysis of aircraft spectrometer data with logarithmic residuals, Proceedings of the Airborne Imaging, Spectrometer Data Analysis Workshop, JPL PUBLICATION 85-41, p. 111-119
- Hu, B., Wang, J. B., Gao, Z. J. and Fang, X. D. (1965)
Some geological problems of the Palaeozoic of the Tarim Basin, Acta Geol. Sinica, 45, (2), P. 131-142 (in Chinese)
- Hunt, G. R., Ed. (1982)
Spectroscopic Properties of Rock and Minerals, In: Handbook of Physical Properties of Rocks, Vol. I, Chapter 3, CRC press, Florida, p. 295-385
- Kruse, F. A. (1988)
Use of Airborne Imaging Spectrometer Data to Map Minerals Associated with Hydrothermally Altered Rocks in the Northern Grapevine Mountain, Nevada, and California, Remote Sensing Environment, 24, p. 31-51
- Nishidai, T. and Berry, J. (1990)
Structure and Hydrocarbon potential of the Tarim Basin (NW China) from Satellite Imagery, Journal of Petroleum Geology, Vol. 13(1), p. 35-58
- Okada, K. and Iwashita, A. (1990)
Hyper-Multispectral Image Analysis Based on Waveform Characteristics of spectral Curve, ADVANCED IN SPACE RESEARCH, Proceedings of the Twenty-Eighth Plenary Meeting held in The Hague, The Netherlands 1990, COSPAR, in press
- Tian, Z., Chai, G. and Lin, L. (1985)
Tectonic evolution of the Tarim Basin and its hydrocarbon potential, Oil and Gas Geol., 6, (3), p. 250-258, (in Chinese)

Acknowledgement

The authors would like to thank Earth Resources Data Analysis Center (ERSDAC) for acceptance of publication and the Chinese Academy of Sciences for their cooperation about the data acquisition and the field survey.

Table 1 Band specification of the GER system.

Wavelength range (nm)	bandwidth (nm)	Number of band
430 - 970	23.4	24
1080 - 1800	120.0	7
1980 - 2500	16.3	32

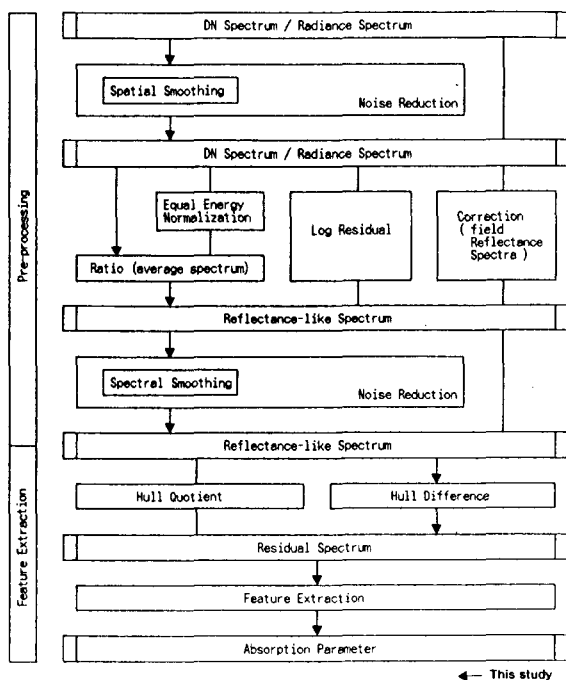


Figure 1 Flow chart of processing.

wavelength : λ
depth : D
area : A
width : $W = A / D \times 2$
symmetry : $S = (A_{left} / A) \times 2 - 1$
slope of hull : $\theta = \tan^{-1} \left(\frac{R_e - R_s}{\lambda_e - \lambda_s} \right)$

Figure 3 Schematic diagram of definition of absorption parameters.

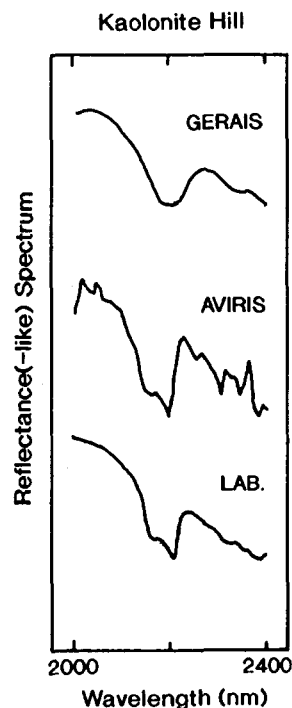
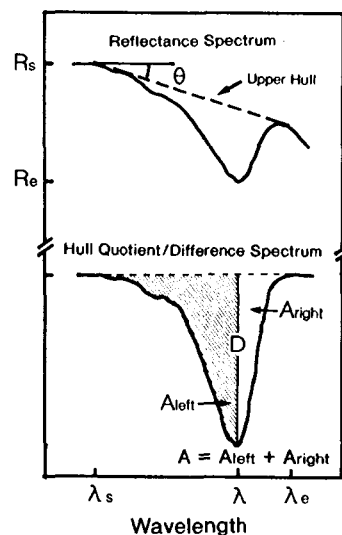


Figure 2

Comparison of a laboratory spectrum of a rock sample collected at Kaolinite Hill and converted spectra of AVIRIS and GERAIS in the corresponding areas.





False Color Image
(187 192 198)

1989 AVIRIS
Cuprite, Nevada
Parameter-image

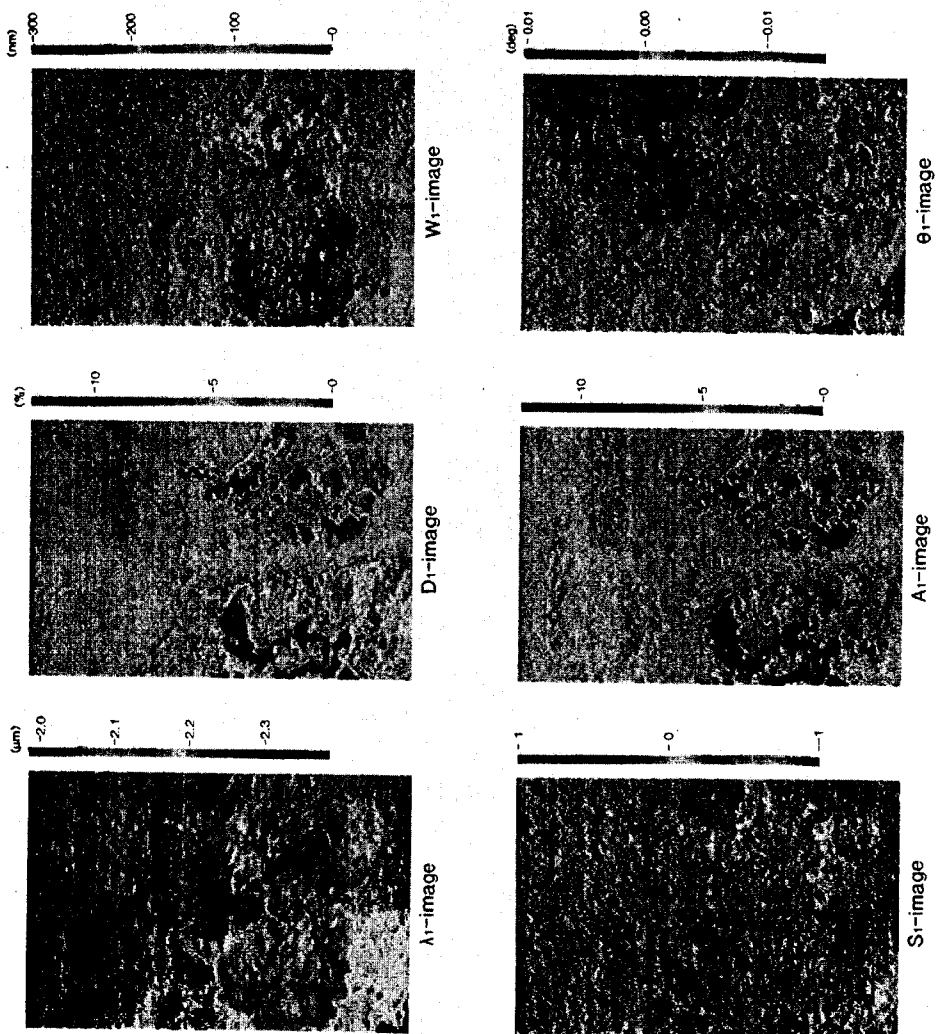


Figure 4
Color-coded parameter-images of AVIRIS for the deepest
absorption (see slide 24).

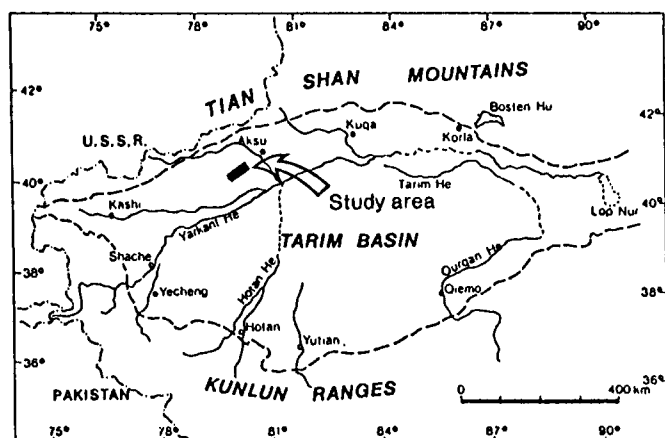



Figure 5 Locality map of the study area.

Period	Group/Formation	Column	Thickness	Lithology
Early Permian	Kaipazileike Fm.		1,200m	dolerite alternation of basalt lava and yellowish grey coarse sandstone
	Kupukuziman Fm.			red - yellowish white sandstone and siltstone coal seam basalt lava
	Kangkelin Fm.		100m 50m	purple - yellowish white sandstone and siltstone limestone including fusuline, coral, crinoid
				coarse sandstone and conglomerate
Devonian	Keziertage Fm.		500 - 900m	lake deposit alternation of purplish brown sandstone, mudstone and siltstone
	Yimuganlaw Fm.			deltaic deposit purplish - red sandstone dominant
Silurian	Tataiertage Fm.			deltaic (shallow marine) deposit
	Kepingtage Fm.		400 - 700m	bluish green sandstone partly including conglomerate, mudstone and siltstone
Ordovician	Yingen Fm.		40m	carbonaceous black shale
	Qilang Fm.			alternation of muddy limestone, limy mudstone and black shale
	Kanlin Fm.			greyish white limestone (including weathered limy deposit)
	Saergen Fm.			carbonaceous black shale grey muddy limestone grey muddy dolomitic limestone (partly saccharoidal)
Cambrian	Qilutige Gr.		800m	
	Awatage Gr.			grey muddy dolomitic limestone stromatolite, algal biscuit
Shen	Shayike Fm.		550m	red mudstone, siltstone
	Wushonggeer Fm.			
	Xiaerbulake Fm.			phosphorite, barite at the base
	Qigebulake Fm.		170m	grey dolomitic limestone, stromatolite
	Supailibulake Fm.			alternation of red sandstone, mudstone and conglomerate

Figure 6 Generalized stratigraphic column of the study area.

FALSE COLOR IMAGE
CH 6, 10, 17

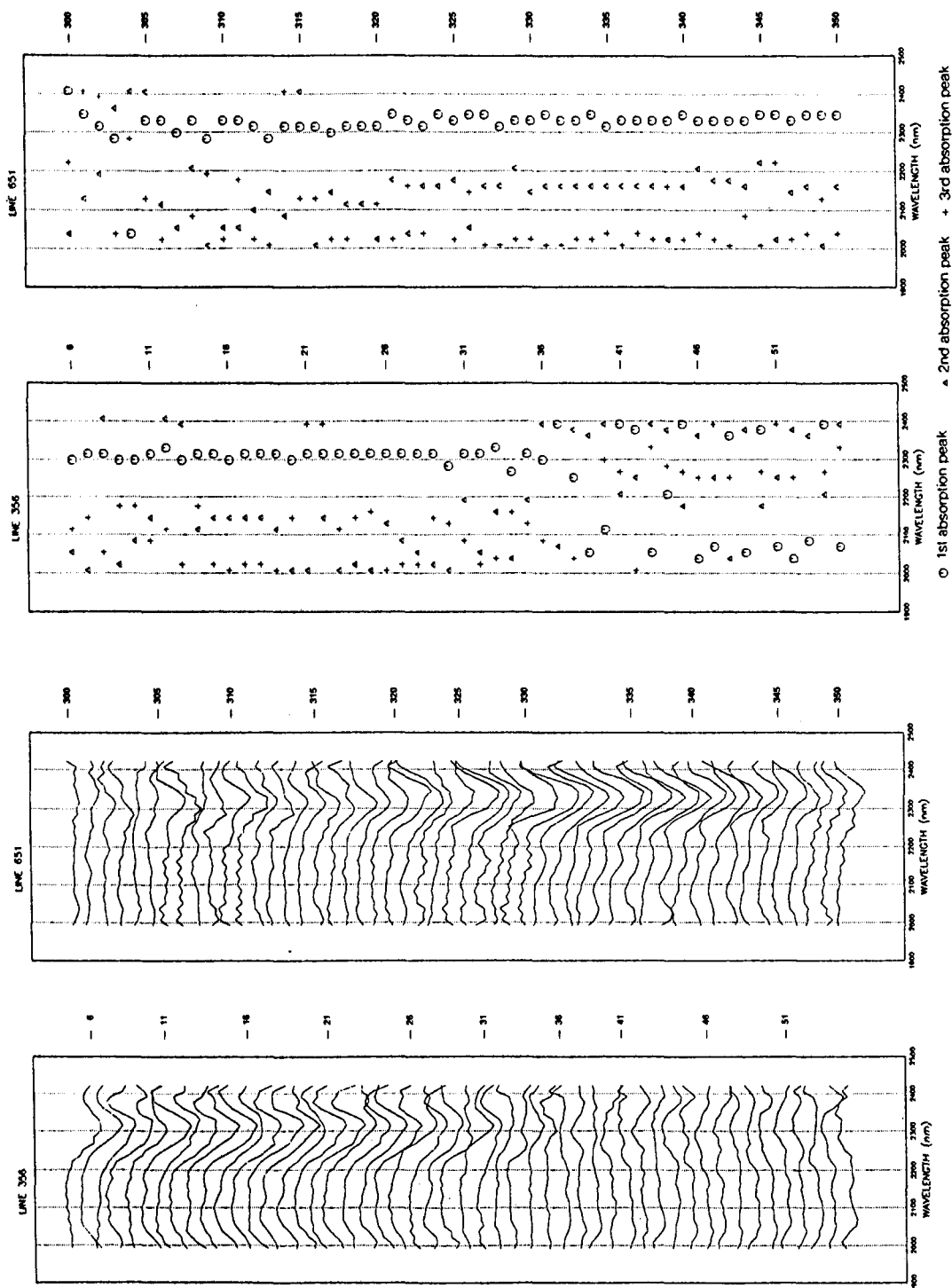
ABSORPTION BAND IMAGE
SUPERIMPOSED ON CH 17

■	CH 41 (2115 NM)
■	CH 42 (2130 NM)
■	CH 43 (2146 NM)
■	CH 44 (2161 NM)
■	CH 45 (2176 NM)
■	CH 46 (2192 NM)
■	CH 47 (2207 NM)
■	CH 48 (2223 NM)
■	CH 49 (2238 NM)
■	CH 50 (2253 NM)
■	CH 51 (2269 NM)
■	CH 52 (2284 NM)
■	CH 53 (2299 NM)
■	CH 54 (2315 NM)
■	CH 55 (2330 NM)
■	CH 56 (2346 NM)
■	CH 57 (2361 NM)
■	CH 58 (2376 NM)



Figure 7 False color image and λ , image superimposed on band 17 for a part of eastern Yingan Shan (see slide 25).



(a)

(b)

Figure 8 Examples of reflectance-like spectra (a) and absorption peaks calculated by the software (b) for image lines in Figure 7.